

ORIGINAL RESEARCH ARTICLE

Mechanisms of Sinoatrial Node Dysfunction in Heart Failure With Preserved Ejection Fraction

Thassio Mesquita¹, PhD*; Rui Zhang, MD*; Jae Hyung Cho, MD, PhD*; Rui Zhang, MD; Yen-Nien Lin², MD, PhD; Lizbeth Sanchez, BS; Joshua I. Goldhaber³, MD; Joseph K. Yu, BS; Jialiu A. Liang, BS; Weixin Liu, BS; Natalia A. Trayanova⁴, PhD; Eugenio Cingolani⁵, MD

BACKGROUND: The ability to increase heart rate during exercise and other stressors is a key homeostatic feature of the sinoatrial node (SAN). When the physiological heart rate response is blunted, chronotropic incompetence limits exercise capacity, a common problem in patients with heart failure with preserved ejection fraction (HFpEF). Despite its clinical relevance, the mechanisms of chronotropic incompetence remain unknown.

METHODS: Dahl salt-sensitive rats fed a high-salt diet and C57Bl6 mice fed a high-fat diet and an inhibitor of constitutive nitric oxide synthase (N^o-nitro-L-arginine methyl ester [L-NAME]; 2-hit) were used as models of HFpEF. Myocardial infarction was created to induce HF with reduced ejection fraction. Rats and mice fed with a normal diet or those that had a sham surgery served as respective controls. A comprehensive characterization of SAN function and chronotropic response was conducted by in vivo, ex vivo, and single-cell electrophysiologic studies. RNA sequencing of SAN was performed to identify transcriptomic changes. Computational modeling of biophysically-detailed human HFpEF SAN was created.

RESULTS: Rats with phenotypically-verified HFpEF exhibited limited chronotropic response associated with intrinsic SAN dysfunction, including impaired β -adrenergic responsiveness and an alternating leading pacemaker within the SAN. Prolonged SAN recovery time and reduced SAN sensitivity to isoproterenol were confirmed in the 2-hit mouse model. Adenosine challenge unmasked conduction blocks within the SAN, which were associated with structural remodeling. Chronotropic incompetence and SAN dysfunction were also found in rats with HF with reduced ejection fraction. Single-cell studies and transcriptomic profiling revealed HFpEF-related alterations in both the “membrane clock” (ion channels) and the “Ca²⁺ clock” (spontaneous Ca²⁺ release events). The physiologic impairments were reproduced in silico by empirically-constrained quantitative modeling of human SAN function.

CONCLUSIONS: Chronotropic incompetence and SAN dysfunction were seen in both models of HF. We identified that intrinsic abnormalities of SAN structure and function underlie the chronotropic response in HFpEF.

Key Words: arrhythmias, cardiac ■ heart failure ■ heart rate ■ sinoatrial node

The positive chronotropic effect of β -adrenergic receptor (β -AR) stimulation on the heart is a physiological response experienced during emotional and physical stressors. Impaired heart rate (HR) response to acute stress (also known as the fight-or-flight response) is manifested in patients with chronotropic incompetence, which has been associated with adverse outcomes and

increased mortality in heart failure (HF) with preserved ejection fraction (EF).^{1,2} However, the mechanisms responsible for chronotropic incompetence in HF with preserved EF (HFpEF) remain unclear. Impaired function of the sinoatrial node (SAN) has been posited in patients with HFpEF,³ but others implicate extrinsic factors (limited biventricular compliance,⁴ impaired vasodilation,¹

Correspondence to: Eugenio Cingolani, MD, Smidt Heart Institute, Cedars-Sinai Medical Center, 127 S San Vicente Blvd, Los Angeles, CA 90048. Email eugenio.cingolani@csmc.edu

*T. Mesquita, R. Zhang, and J.H. Cho contributed equally.

Supplemental Material is available at <https://www.ahajournals.org/doi/suppl/10.1161/circulationaha.121.054976>.

For Sources of Funding and Disclosures, see page 58.

© 2021 American Heart Association, Inc.

Circulation is available at www.ahajournals.org/journal/circ

Clinical Perspective

What Is New?

- We identified latent sinoatrial node dysfunction in heart failure with preserved ejection fraction (HFpEF) that can be unmasked under stress testing.
- Our integrated approach revealed functional, structural, and molecular features underlying the defective sinoatrial node function in HFpEF.
- Although transcriptomic profiling reveals changes in multiple disease-associated genes, depressed “membrane clock” and “Ca²⁺ clock” components are closely linked to the impaired sinoatrial node function.

What Are the Clinical Implications?

- Provocative testing can be valuable to elicit functional abnormalities to facilitate HFpEF diagnosis.
- Considering the exceptionally high clinical and epidemiological convergence between atrial fibrillation and HFpEF, sinoatrial node dysfunction may underlie the development of abnormal atrial rhythms in HFpEF.

elevated pulmonary pressure,⁵ and other peripheral and autonomic abnormalities⁶). SAN dysfunction has been extensively studied in other diseases,^{7,8} including chronic HF with reduced EF (HFrEF),^{9,10} establishing the foundation for theories on the mechanisms of SAN arrhythmias.^{7,11} Moreover, SAN dysfunction facilitates the development of atrial fibrillation,¹² a rhythm disorder associated with HFpEF.¹³

We hypothesized that SAN dysfunction underlies chronotropic incompetence in HFpEF. To investigate the role of the intrinsic cardiac pacemaker on chronotropic incompetence in HFpEF, we performed extensive SAN phenotyping (both at baseline and after stress) in the well-characterized Dahl salt-sensitive (DSS) rat model of HFpEF. This model has features reminiscent of human HFpEF, including: (1) signs of HF with no decline in global systolic function¹⁴; (2) comorbidities including hypertension, insulin resistance, and hyperlipidemia^{15,16}; and (3) adverse electric remodeling with high incidence of sudden death.^{17,18} Given the heterogeneity of HFpEF subphenotypes and the variety of comorbidities in human HFpEF, the main findings were validated in the 2-hit HFpEF mouse model.^{19–21}

METHODS

The data, analytical methods, and study materials will be made available to other researchers by reasonable request to the corresponding author for the purposes of reproducing results or replicating procedures. Descriptions and sources of reagents and an expanded [Methods](#) section are provided

in the [Supplemental Material](#). All animal procedures were reviewed and approved by the Institutional Animal Care and Use Committee of Cedars-Sinai Medical Center.

Statistical Analysis

Pooled data are expressed as mean±SEM. Statistical comparisons were performed using GraphPad Prism 9 (San Diego, CA). Differences between groups were tested using a 2-tailed unpaired Student *t* test, or where repeated measures were necessary, either repeated measures ANOVA or mixed-effect model was used for occurrences of missing data. Post hoc pair-wise testing was Bonferroni-corrected for multiple comparisons. Proportions were tested using the Fisher exact test. Kaplan–Meier analysis was used for survival rates with the log-rank test. *P* < 0.05 was considered statistically significant.

RESULTS

Exercise Intolerance and Chronotropic Incompetence of HFpEF Are Associated With Lower β-AR Responsiveness

DSS rats fed a high-salt diet developed phenotypic changes of HFpEF.¹⁷ The experimental timeline is shown in Figure 1A. All animals underwent initial screening by echocardiography ([Table S1](#)). Between 14 and 18 weeks (Figure 1B), EF remained unchanged in high-salt diet-fed DSS rats compared with those fed a normal-salt diet (control). In contrast, analysis of E- and A-waves from pulse-wave Doppler mode and E'- and A'-wave changes in tissue Doppler showed diastolic dysfunction as evidenced by decreased E/A ratio (Figure 1C) and increased E/E' ratio (Figure 1D). Hypertension, which is one of the most prevalent comorbidities in human HFpEF,² was developed in high-salt diet-fed DSS animals (Figure 1E). Importantly, high-salt diet-fed DSS animals exhibited signs of HF (eg, weakness, decreased mobility, labored breathing, and/or body edema), as indicated by the elevated HF score in Figure 1F. Rats with HF signs and echo-verified diastolic dysfunction (and preserved EF) were diagnosed with HFpEF and used for experiments discussed hereafter. Pulmonary congestion was verified by increased lung weight/tibia length ratio in HFpEF animals compared with controls ([Figure S1](#)).

To assess the chronotropic reserve, we used cardiopulmonary exercise stress testing. Despite no changes in baseline HR, all animals presented an increase in HR at maximal exercise capacity (Figure 1G and 1H). However, HFpEF animals showed a significantly smaller increase in the maximal HR compared with control animals (Figure 1G and 1H), indicative of chronotropic incompetence. Exercise intolerance was observed in HFpEF animals (Figure 1H, inset), similar to that seen in HFpEF patients.¹ Although the reduced functional capacity may limit the maximal HR response to exercise (Figure 1I), impaired HR regulation may also occur after exercise cessation.²² In control animals, typical postexercise HR

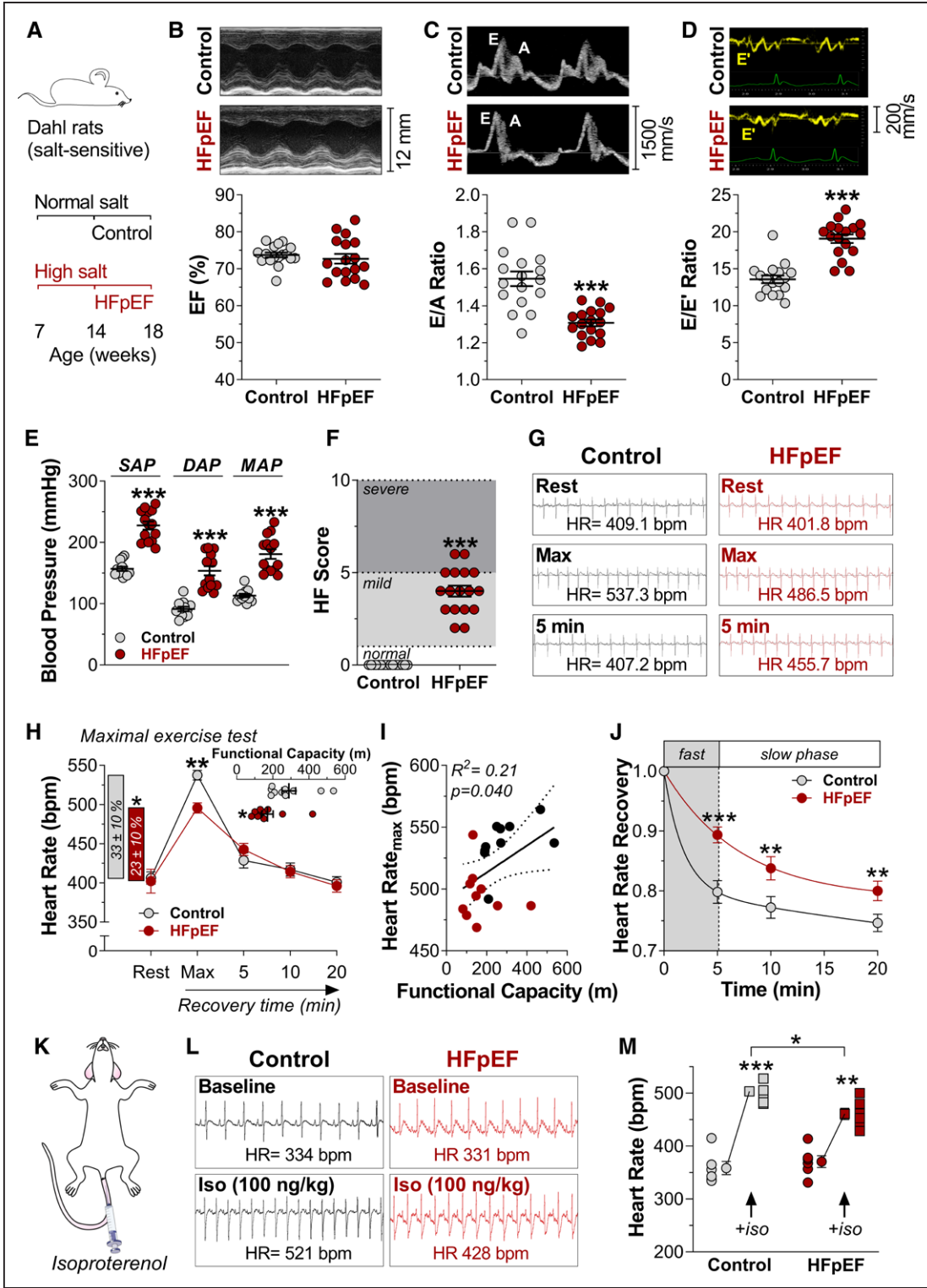


Figure 1. Cardinal exercise intolerance and chronotropic incompetence of HFpEF phenotyping are associated with lower β -adrenergic receptor responsiveness. **A**, Experimental design. Dahl salt-sensitive rats were maintained on normal-salt (0.4%) or high-salt (8%) dietary regimens from 7 weeks of age and HFpEF verified between 14 to 18 weeks old. **B**, Representative left ventricular M-mode echocardiographic images (top) of EF analysis (bottom). **C**, Representative images (top) of pulse-wave Doppler showing E (early filling)– and A (atrial filling)–wave changes (bottom). **D**, Representative images (top) of tissue Doppler describing E'– and A'–wave changes (bottom). **E**, Noninvasive blood pressure measurements. **F**, Heart failure score defined by the following parameters: appearance, breathing, mobility, edema, and weight. (Continued)

Figure 1 Continued. **G**, Representative telemetry ECG recordings. **H**, Resting, maximal, and recovery of HR in response to exercise test (inset, functional capacity measured as the total running distance). $n=10$ animals in each group. **I**, Relationship between functional capacity and maximal HR response (Pearson coefficient). Data are fit by linear regression; dashed lines represent 95% CI. **J**, HR recovery time after the maximal exercise test, data are fit by 2 exponential decay. **K**, In vivo isoproterenol stress testing was used to determine the chronotropic reserve. **L**, Representative ECG recordings. **M**, Quantification of β -adrenergic-induced heart rate increase. Data are expressed as mean \pm SEM. Unpaired Student *t* test (**B–F**, **H**, insets). Repeated measures ANOVA followed by Bonferroni post hoc test (**H**, **J**, and **M**). * $P<0.05$; ** $P<0.01$; *** $P<0.001$. DAP indicates diastolic arterial pressure; EF, ejection fraction; HFpEF, heart failure with preserved ejection fraction; HR, heart rate; ISO, isoproterenol; MAP, mean arterial pressure; and SAP, systolic arterial pressure.

recovery was shown with 2 distinct phases: the first, a fast phase characterized by exponential HR recovery—mainly because of parasympathetic reactivation—followed by the second, a slow component characterized by a gradual decay of HR as the result of the sympathetic withdrawal (Figure 1J). The prolonged HR recovery after exercise in HFpEF revealed 2 subtypes of chronotropic incompetence: (1) submaximal peak of HR (Figure 1G and 1H); and (2) inadequate HR recovery (Figure 1J). To exclude potential interference of limited functional capacity from the chronotropic response, we carried out an in vivo pharmacological stimulation test with isoproterenol, a nonselective agonist of β -AR (Figure 1K). Validating our exercise findings, HFpEF animals had a lower chronotropic response to β -AR stimulation compared with controls (Figure 1L and 1M). To study the potential impact of chronotropic response on cardiac output, we performed a dobutamine stress echocardiogram on control and HFpEF rats. Importantly, HFpEF rats presented inadequate cardiac output reserve in response to dobutamine infusion (Figure S2).

Given the heterogeneity of HFpEF subphenotypes, we also conducted experiments using the recently described 2-hit mouse model.¹⁹ Mice concomitantly fed with a high-fat diet (metabolic hit) and nitric oxide synthase inhibitor (hypertensive hit) manifested increased left ventricular filling pressures and preserved EF as measured by noninvasive echocardiogram (Figure S3A–S3D; Table S2), elevated systemic blood pressure (Figure S3E), and increased lung weight/tibia length ratio (Figure S3F). Although no statistical differences were seen at baseline or maximal HR in HFpEF mice compared with controls, the fractional increase in HR in HFpEF mice was significantly smaller (Figure S3G). Limited exercise tolerance (Figure S3G, inset) and delayed postexercise HR recovery (Figure S3H) were also seen in HFpEF animals. Our findings in 2 different models of HFpEF demonstrated exercise intolerance and limited chronotropic response, mirroring the clinical features of human HFpEF. Although both HFpEF models showed an inadequate cardiac output response to dobutamine (Figure S4), the impaired chronotropic response was the major driver in DSS HFpEF rats (Figure S2), while a marginal increase in stroke volume appeared to be the main factor in HFpEF mice (Figure S4).

To elucidate whether our findings were unique to HFpEF, we characterize them in a previously established model of HFrEF.⁹ Rats with characteristic signs of HF

and reduced EF (<45%) were referred to as HFrEF (Figure S5A–S5C) and compared with controls (Table S3). Despite the significant change of absolute HR in response to exercise in HFrEF compared with controls (Figure S5D), the fractional increase was similar between groups. HFrEF rats also presented reduced exercise capacity (Figure S5D, inset) and delayed postexercise HR recovery (Figure S5E). Accordingly, as previously seen in HFrEF patients,¹⁰ corrected SAN recovery time (cSNRT) was prolonged in HFrEF rats compared with controls (Figure S5F). Moreover, limited chronotropic response to in vivo β -AR stimulation was observed in HFrEF rats (Figure S5G). In summary, most of the functional changes in SAN function and exercise capacity observed in both models of HFpEF were not exclusive of this condition, and were also seen in rats with HFrEF.

Impaired SAN β -AR Responsiveness Reveals Uncoordinated Recruitment of Pacemaker Clusters Favoring Rhythmic Abnormalities

Autonomic imbalance, which contributes to impaired chronotropic response, has been described in human HFpEF.¹ To exclude a contribution from autonomic innervation in vivo, we optically mapped an intact SAN/atrial preparation ex vivo. Figure 2A shows that the functional and anatomic boundaries of the rat SAN are similar to those of the human SAN.²³ Representative activation maps demonstrate that, under spontaneous sinus rhythm, the earliest activation site is located at the right atrial posterior wall, which anatomically corresponds to the location of the SAN (Figure 2A). In concordance with our in vivo findings (Figure 1K–1M), a blunted beating rate response to β -AR stimulation was also evident in isolated SAN tissue from HFpEF rats compared with controls (Figure 2B). Given the fact that β -AR isoforms and GRKs (G protein-coupled receptor kinases) work in concert to desensitize, internalize, and ultimately down-regulate β -AR in HFrEF ventricular myocardium,²⁴ we next evaluated the abundance of these key proteins in the SAN. Neither mRNA nor protein expression of β -AR isoforms (β_1 and β_2) were changed in the SAN of HFpEF rats compared with controls (Figure S6A and S6B). Moreover, no significant changes were observed in the protein expression of cardiac isoforms of GRKs (GRK2 and GRK5) or phosphorylation levels in the activating site of GRK2^{ser670} (Figure S6B). In accordance with the rat HFpEF model, SAN/atrial preparation from

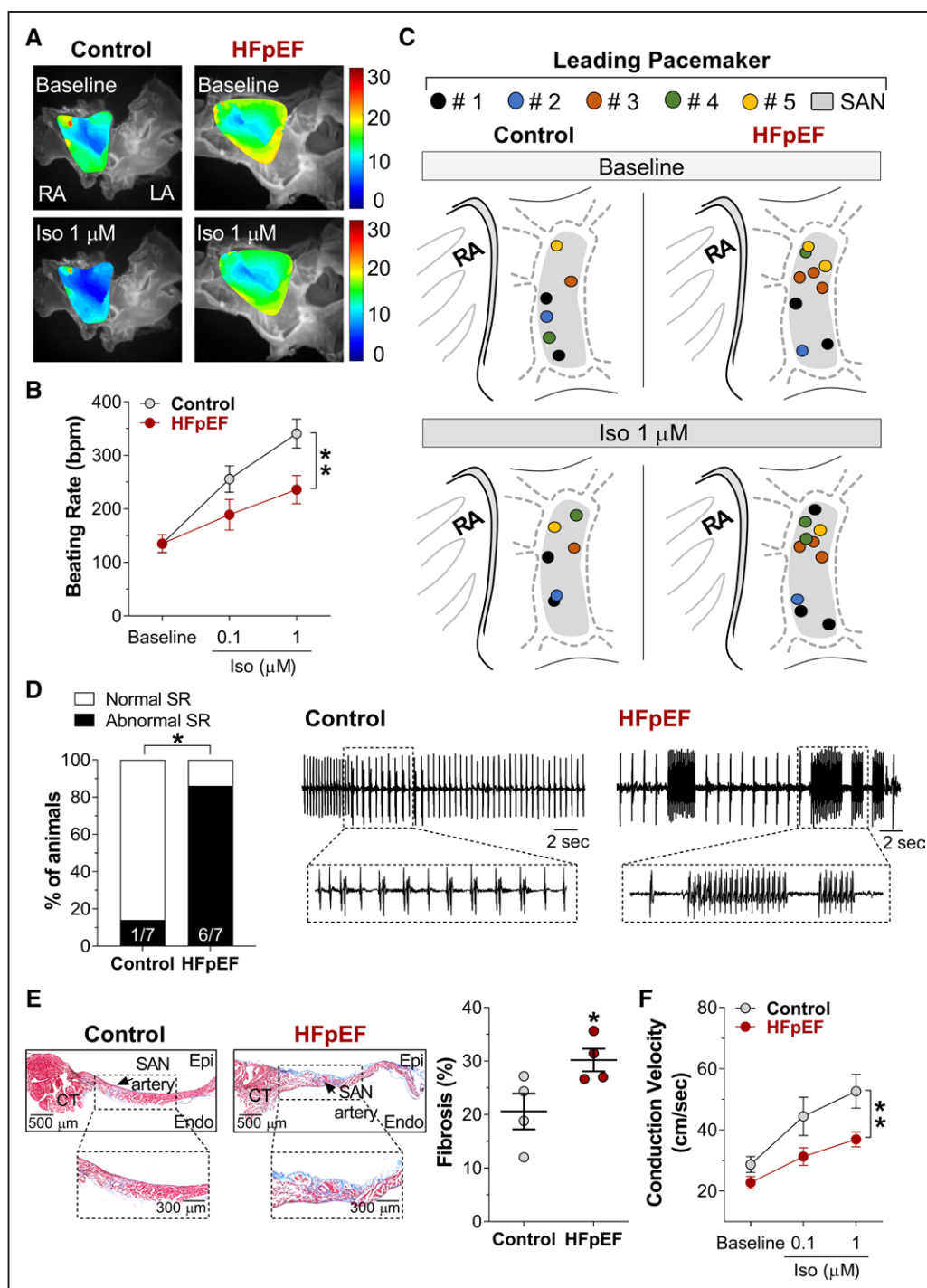


Figure 2. Impaired SAN β -adrenergic receptor responsiveness reveals uncoordinated recruitment of pacemaker clusters favoring rhythmic abnormalities.

A, Representative images of isochronal voltage maps under spontaneous SR and Iso stimulation. **B**, Spontaneous SR and concentration–response curve for Iso were used to evaluate ex vivo beating rate; $n=7$ animals in each group. **C**, Locations of the SAN leading pacemaker (dots), defined as the earliest activation site, and the effects of β -adrenergic stimulation on the leading pacemaker site location. Each colored dot represents an estimated location from 5-s recordings from an animal replicate replotted onto a schematic SAN region. **D**, Occurrence of abnormal SR throughout the dose–response curve to Iso (**left**) and representative electrogram traces (**right**). **E**, Representative Masson trichrome–stained sections of SAN (**left**) and quantification (**right**). **F**, Conduction velocity within the SAN region at spontaneous SR and concentration–response curve for Iso. Data are expressed as mean \pm SEM. Repeated measure ANOVA followed by Bonferroni post hoc test (**B** and **F**). Fisher exact test (**D**). Unpaired Student t test (**E**). * $P<0.05$; ** $P<0.01$. CT indicates crista terminalis; Epi, epicardium; Endo, endocardium; HFpEF, heart failure with preserved ejection fraction; Iso, isoproterenol; LA, left atria; RA, right atria; SAN, sinoatrial node; and SR, sinus rhythm.

phenotypically verified 2-hit HFpEF mice presented an attenuated beating rate in response to isoproterenol (Figure S7A), compared with controls. The presence of an oscillatory leading pacemaker site (Figure S7B; Video S1), irregular beating rate, and conduction blocks were also observed (Figure S7C).

To functionally characterize the activation pattern of the SAN in both experimental groups, high-resolution optical mapping was performed (Figure 2C). Although 1 control SAN preparation displayed 2 competing activation sites, the remaining samples had a single coordinated leading pacemaker focus. β -AR stimulation slightly shifted the leading pacemaker toward the superior aspect within the SAN area. Conversely, even at baseline, multiple disorganized leading pacemaker sites were observed in HFpEF SAN preparations, while β -AR stimulation failed to shift and resynchronize the leading pacemakers (Figure 2C). In concordance with the chaotic activation pattern, 85% of HFpEF SAN preparations developed irregular rhythms (eg, atrial bigeminy, sinus arrest, tachybradycardia, and atrial fibrillation) on isoproterenol stimulation identified by field atrial/SAN electrogram (Figure 2D). By contrast, only 1 control SAN preparation displayed a brief bigeminy episode, while most of the controls sustained high beating rates under coordinated sinus rhythm (Figure 2D).

The SAN is almost entirely insulated from the surrounding atria by fibrosis, fat, and discontinuous myofibers.²⁵ Masson trichrome staining distinguished the SAN region surrounding the SAN artery from the neighboring atria (Figure 2E). Increased SAN fibrosis was observed in HFpEF SAN compared with controls (Figure 2E). Although fibrotic remodeling of SAN can impact electric conduction,²⁶ no significant change in conduction velocity within the SAN region was observed between groups at baseline (Figure 2F). However, after β -AR stimulation, a dose-dependent increase in beating rate, supported by faster electric impulse propagation, was seen in controls but not in HFpEF SAN preparations (Figure 2F). Taken together, this shows that impaired chronotropic response is associated with the presence of multiple intranodal pacemakers, revealing a distinctive pattern of intrinsic SAN dysfunction in HFpEF.

Adenosine Challenge Reveals Areas of SAN Exit Block

Intracardiac programmed electric stimulation was used to measure the cSNRT as a measure of in vivo SAN function (Figure 3A and 3B). Supporting our hypothesis of impaired SAN function, Figure 3C shows prolonged cSNRT in HFpEF animals compared with controls. Circadian HR oscillation shows similar diurnal variation, as well as narrower HR variability, during the nocturnal period in HFpEF compared with control animals (Figure 3D), supporting the autonomic dysfunction previously report-

ed in both humans and animal models.^{1,18} While these HFpEF changes are associated with increased mortality (Figure 3E), it is important to point out that the overall mortality reported here includes not only sudden death (as we previously reported¹⁸), but also that attributed to following protocol-mandated euthanasia criteria because of severe distress in the animals.²⁷

Given previous results, we tested the SAN function in an intact ex vivo atrial/SAN preparation.²³ Optical maps during pacing-induced suppression of sinus rhythm led us to identify areas of dysfunction within the SAN and the presence of conduction blocks. Substantiating our in vivo findings, we also found longer cSNRT in HFpEF SAN compared with controls (Figure 3F). In concordance with our findings in the DSS rat HFpEF model, atrial/SAN preparation from 2-hit HFpEF mice presented longer cSNRT compared with controls (Figure S7D). We further stressed the rat SAN by exposure to adenosine (1 μ mol/L, as complete SAN arrest can be seen at higher concentrations²³). As expected, adenosine-induced suppression of SAN automaticity was observed by a reduction of the intrinsic beating rate in both groups. However, cSNRT was longer in HFpEF, while remaining unchanged in control SAN tissue (Figure 3F). Using our integrated mapping approach, we mapped several regions of SAN conduction pathways responsible for the conductivity of electric impulses to the right and left atria.^{7,23,28} Interestingly, no conduction block was detected in control samples exposed to adenosine; however, an interatrial block was observed in 67% of HFpEF samples (Figure 3G). These results indicate that HFpEF animals have a vulnerable SAN fail-safe mechanism for automaticity and conduction in response to stressors.

Suppressed Membrane Clock in HFpEF SAN

To explore the molecular basis of the SAN dysfunction in HFpEF rats, we performed next-generation RNA sequencing in isolated SAN tissue. SAN specificity was verified by sequencing SAN and atrial tissue from control rats. Accordingly, control SAN tissue presented higher levels of *Hcn4* (hyperpolarization-activated cyclic nucleotide-sensitive isoform 4), *Shox2* (short stature homeobox 2), and *Tbx3* (T-box transcription factor 3) compared with atrial tissue (Figure S8A), confirming enriched molecular markers of SAN. RNA sequencing revealed changes in the expression of 835 genes in HFpEF SAN compared with controls (635 upregulated and 200 downregulated; Table S4). Taking into consideration recent studies profiling the molecular signatures of different cell types that populate the SAN at the embryonic stage,^{29,30} we only observed a significant loss of *Igf1bp5* (insulin-like growth factor binding protein 5) and *Hcn4* (belonging to compact SAN) in HFpEF SAN, without enrichment of transitional/atrial-like genes (Figure S8B). Thus, these

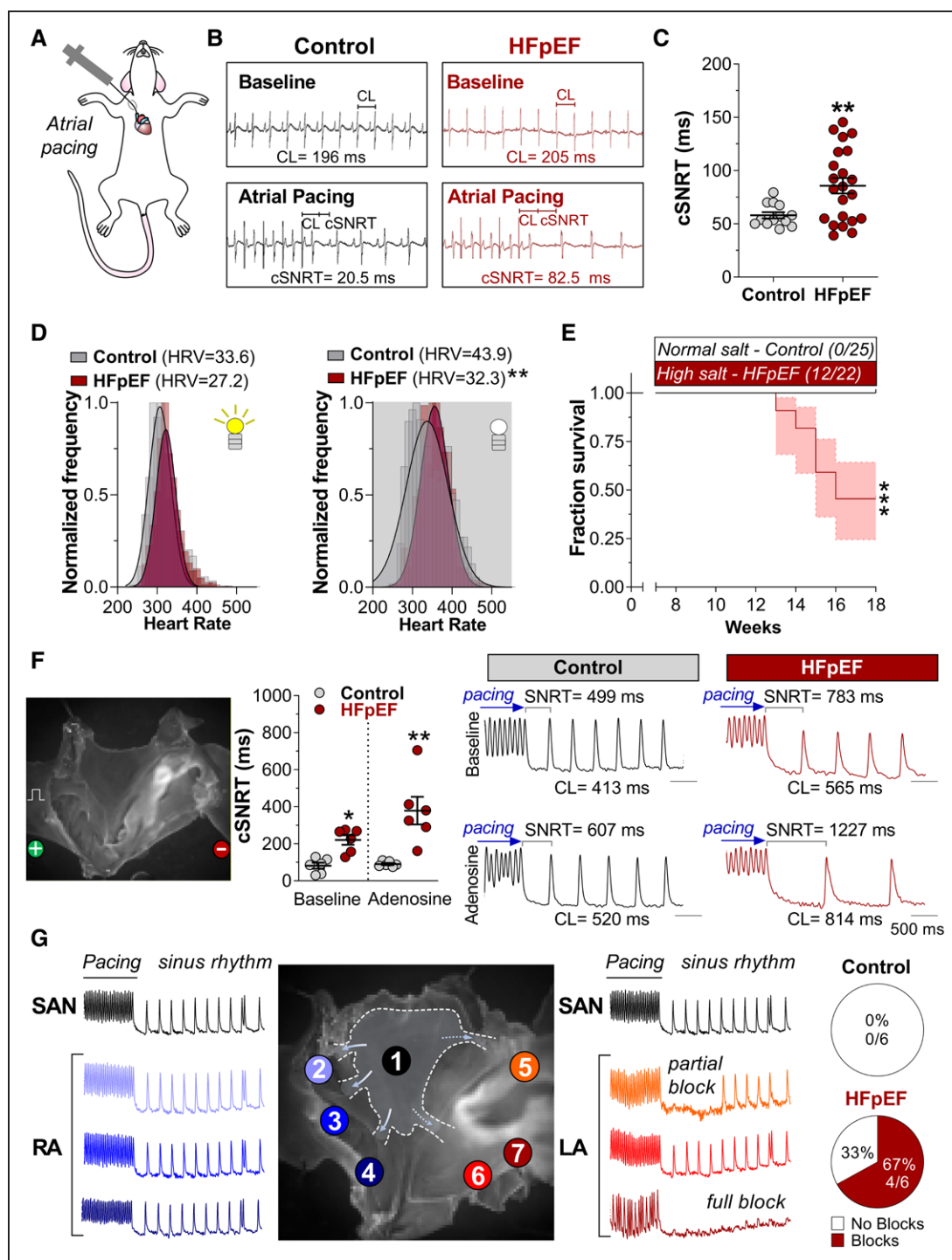


Figure 3. Unmasked SAN dysfunction by adenosine challenge reveals conduction block.

A, Intracardiac electrophysiology study was used to determine the SAN function. **B**, Representative ECG recordings. **C**, Quantification of cSNRT time (corrected by intrinsic CL). **D**, Histogram of the circadian oscillation of heart rate during day (left) and night (right). Individual standard deviation of heart rate was used as a measure of HRV; n=10 animals in each group. **E**, Survival analysis of control and HFpEF rats to 18 weeks of age. **F**, Representative image of electrodes placement surrounding the ex vivo SAN/atrial tissue loaded with a voltage-sensitive dye (left). Overdriving suppression of SAN for assessing the cSNRT was achieved by rapid pacing from the RA. cSNRT was quantified before (baseline) and after treatment with adenosine (1 μ mol/L) for 10 min (middle). Representative optical action potential traces during RA pacing and time taken to recover the sinus rhythm (right). **G**, Overview of HFpEF SAN maps uncover the presence of conduction blocks. Data are expressed as mean \pm SEM. Unpaired Student *t* test (**C** and **D**). Log-rank test (**E**). Repeated measures ANOVA followed by Bonferroni post hoc test (**F**). Fisher exact test (**G**). **P*<0.05; ***P*<0.01; ****P*<0.001. CL indicates cycle length; cSNRT, corrected sinoatrial node recovery time; HFpEF, heart failure with preserved ejection fraction; HRV, heart rate variability; Iso, isoproterenol; LA, left atrium; RA, right atrium; SAN, sinoatrial node; and SNRT, sinoatrial node recovery time.

findings do not indicate a molecular shift toward a less nodal phenotype in HFpEF SANs.

Ingenuity Pathway Analysis was performed to investigate the upregulated and downregulated canonical pathways (Figure 4A; Table S5). Along with these findings, gene ontology analysis revealed that SAN dysfunction in HFpEF animals was associated with significant enhancement of multiple disease-associated genes, including those related to inflammation, extracellular matrix remodeling, and metabolic pathways (Table S6). To verify whether the transcriptome changes align with the available human database, further Ingenuity Pathway Analysis in silico analysis was used. By objectively filtering our analysis to the tissue type and disease, the closest related disease to SAN dysfunction was sick sinus syndrome. As highlighted in the volcano plot, among the 5 potential genes related to human sick sinus syndrome (*Hcn4*, *Cacna1d* [calcium voltage-gated channel subunit $\alpha 1D$], *Myh6* [myosin heavy chain 6], *Snta1* [syntrophin $\alpha 1$], and *Scn5a* [sodium voltage-gated channel α subunit 5]), there were 2 (*Hcn4* and *Cacna1d*) significantly downregulated in the HFpEF SAN transcriptome compared with control samples (Figure 4B). A comprehensive representation of differential expression of membrane and Ca^{2+} clock genes in HFpEF SAN is shown in Figure S9. RNA sequencing data have been deposited in the National Center for Biotechnology Information's Gene Expression Omnibus (accession No. GSE184120).

Next, we probed selected proteins to validate our RNA sequencing data. In agreement, we found a decrease in protein levels of $Ca_v1.3$ ([calcium channel, voltage-dependent, L-type, $\alpha 1D$ subunit] encoded by *Cacna1d* gene; Figure 4C). To assess the functional implications of these findings, we then assessed the Ca^{2+} current in isolated SAN cells, which revealed the typical spindle-shaped morphology of pacemaker cells with absent (or poorly present) t-tubules (Figure 4D). We consistently observed reduced L-type Ca^{2+} currents in HFpEF cells compared with controls (Figure 4E and 4G). No changes in cell capacitance were observed between groups (Figure 4F). Although 2 distinct L-type Ca^{2+} channels are expressed in the SAN— $Ca_v1.2$ ([calcium channel, voltage-dependent, L-type, $\alpha 1C$ subunit] encoded by *Cacna1c* [calcium voltage-gated channel subunit $\alpha 1C$]) and $Ca_v1.3$ (the most predominant isoform in SAN cells³¹)— $Ca_v1.2$ expression remained unchanged between groups (Figure S10C). The contribution of T-type Ca^{2+} channels, mainly $Ca_v3.1$ (calcium channel, voltage-dependent, T-type, $\alpha 1g$ subunit; encoded by *Cacna1g* [calcium voltage-gated channel subunit $\alpha 1g$]), has also been demonstrated in pacemaker cells.³² In our study, we found $Ca_v3.1$ expression in SAN tissue (Figure S10A) and patch-clamp studies carried out in control SAN cells revealed an expected leftward shift of the current–voltage relationship, peaking at a more hyperpolarized voltage (-30 mV) compared with L-type Ca^{2+} current (peak at 0 mV; Figure S10B). Interestingly, T-type Ca^{2+}

current density was 23-fold smaller than L-type, thereby indicating a minor contribution of T-type Ca^{2+} current in rat pacemaker cells, as also described in different species.³³ To obtain insights into the contribution of L-type Ca^{2+} channels to the lower chronotropic reserve of HFpEF rats, we stimulated SAN cells with isoproterenol ($1 \mu\text{mol/L}$). Although the peak current in HFpEF SAN cells (after isoproterenol stimulation) was smaller than in controls, the fractional increase of Ca^{2+} current on isoproterenol stimulation was similar between groups (Figure 4H). Despite these changes, the maximal diastolic membrane potential remained unchanged between groups (Figure S11).

Hcn4 is another critical component of the pacemaker function and is indicated as a potential player in the SAN dysfunction in HFpEF animals. As shown in Figure 4I, a decrease in the *Hcn4* protein content of SAN from HFpEF rats compared with controls largely correlated with the dramatic reduction in whole-cell I_f conductance (Figure 4J and 4K). No changes were observed at relevant diastolic membrane potentials (-60 to -30 mV; Figure 4K, inset). Moreover, the lack of change on I_f density on isoproterenol stimulation reveals a perturbed I_f modulation by β -AR stimulation in SAN from HFpEF animals (Figure 4L). Although decreased I_{CaL} and I_f densities were found in SAN cells from 2-hit HFpEF mice compared with controls (Figure S12A and S12B), these changes were modest compared with those seen in HFpEF rats.

Compromised Intracellular Ca^{2+} Transients in HFpEF SAN

Several mechanisms account for the automaticity of pacemaker cells, including the interdependency of the membrane and Ca^{2+} clocks,³⁴ the latter being the intracellular Ca^{2+} release governed by ryanodine receptors and the electrogenic Na^+/Ca^{2+} exchanger (NCX).^{11,35} Thus, we characterized Ca^{2+} transients in SAN cells within the intact tissue loaded with a Ca^{2+} indicator using a high-speed 2D confocal microscopy. Figure 5A represents time-course images of automatic Ca^{2+} transients within the intact SAN. In control, rhythmic Ca^{2+} transients occurred simultaneously throughout the entire SAN (Video S2). Interesting, even under baseline condition, dysrhythmic cells with Ca^{2+} waves, surrounded by rhythmic cells, were observed in random regions within the primary SAN region from HFpEF (Figure 5B; Video S3), while β -AR stimulation led to aberrant sinus rhythm only in HFpEF SAN (Video S4).

To investigate whether Ca^{2+} handling is affected in the SAN of HFpEF animals, the membrane potential of isolated SAN cells loaded with a Ca^{2+} indicator was voltage-clamped at -60 mV to minimize any contribution of the membrane clock. Triggered action potentials (0 mV square voltage pulses at 1 Hz) demonstrate similar steady-state twitch Ca^{2+} transient amplitude at baseline between groups (Figure 5C and 5D). Unchanged

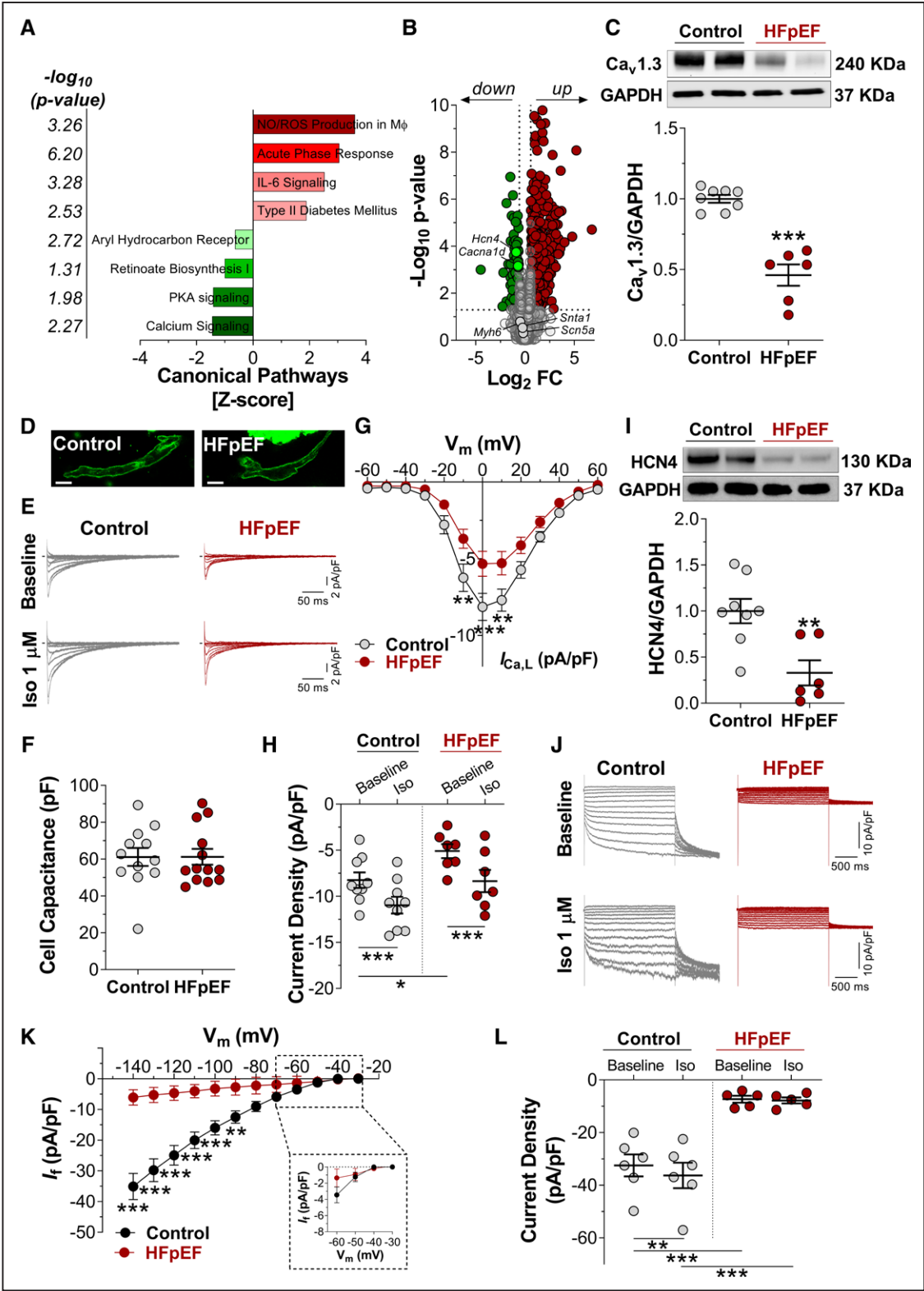


Figure 4. Transcriptome profiling of HFpEF SAN identifies multiple disease-associated mechanisms underpinning depressed membrane clock.
A, Enriched upregulated and downregulated canonical pathways. **B**, Volcano plot of fold change relative to control SAN. Highlighted genes indicate the potential genes related to human sick sinus syndrome, as predicted by in silico analysis; n=4 samples each group. **C**, Representative Western blot images (top) and quantification of $Ca_v1.3$ (encoded by *Cacna1d* [calcium voltage-gated channel subunit $\alpha1D$]) protein expression (bottom). **D**, Representative isolated SAN cells loaded with the voltage dye show the typical spindle shape of pacemaker cells with absent T-tubules (scale bar, 10 μ m). **E**, Representative L-type Ca^{2+} channel currents recorded in isolated SAN cells. **F**, Cell capacitance. (Continued)

Figure 4 Continued. **G**, Average peak current density–voltage relationship of I_{CaL} in control ($n=9$ cells from 3 animals) and HFpEF ($n=7$ cells from 3 animals). **H**, Peak current at 0 mV in the absence or presence of Iso 1 $\mu\text{mol/L}$. **I**, Representative Western blot images (**top**) and quantification of Hcn4 protein expression (**bottom**). **J**, Representative time courses of I_f funny current recorded in isolated SAN cells. **K**, Average peak current density–voltage relationship of I_f in control ($n=6$ cells from 3 animals) and HFpEF ($n=5$ cells from 3 animals; **bottom**), inset highlights no difference in I_f current density between -60 and -30 mV. **L**, Peak current at -140 mV in the absence or presence of Iso 1 $\mu\text{mol/L}$. Data are expressed as mean \pm SEM. Statistical significance was determined using an unpaired Student t test (**C**, **I**, and **F**). **G**, Mixed-effect model with Bonferroni post hoc test. **H**, **K**, and **L**, Repeated measures ANOVA followed by Bonferroni post hoc test. * $P<0.05$; ** $P<0.01$; *** $P<0.001$. $Ca_v1.3$ indicates calcium channel, voltage-dependent, L-type, $\alpha 1D$ subunit; FC, fold change; HCN4, hyperpolarization-activated cyclic nucleotide-sensitive isoform 4; HFpEF, heart failure with preserved ejection fraction; IL-6, interleukin 6; Iso, isoproterenol; Myh6, myosin heavy chain 6; NO/ROS, nitric oxide/reactive oxygen species; PKA, protein kinase A; SAN, sinoatrial node; Scn5a, sodium voltage-gated channel α subunit 5; Snta1, syntrophin $\alpha 1$; and V_m , membrane potential.

Ca^{2+} transient amplitude may reflect the role of $Ca_v1.2$ in maintaining the bulk of Ca^{2+} in the SAN, as proposed.³⁶ Considering that Ca^{2+} handling is affected by a frequency-dependent mechanism,³⁷ and the fact that HFpEF animals have a lower response to isoproterenol, Ca^{2+} transients were assessed at a constant beating rate (Figure 5C and 5D). Elevation of Ca^{2+} transient amplitude was observed in control SAN on β -AR stimulation, while no significant change was found in HFpEF SAN cells (Figure 5C and 5D). Cytosolic Ca^{2+} removal, measured as the Ca^{2+} transient decay time, was similar between groups at baseline (Figure 5E). However, the enhancement of Ca^{2+} reuptake on β -AR stimulation was only observed in control cells; Ca^{2+} reuptake remained unchanged in HFpEF SAN cells (Figure 5E). We then checked the sarcoplasmic reticulum Ca^{2+} load and Ca^{2+} extrusion by applying a rapid caffeine-induced Ca^{2+} release, which activates Ca^{2+} extrusion via I_{NCX} (Figure 5F). No significant changes were observed in the SR Ca^{2+} content (Figure 5G) and I_{NCX} between groups (Figure 5H), as also observed in chronic HF.^{37,38}

Computational Modeling of Biophysically-Detailed Human HFpEF SAN Model

Last, our experimental findings regarding the membrane clock and Ca^{2+} clock remodeling in HFpEF were integrated into a quantitative human SAN model³⁹ (Figure 6A). Without isoproterenol, HFpEF SAN models exhibited identical spontaneous action potential morphology, and beating rate compared with controls (Figure 6B). In contrast, all HFpEF models exhibited submaximal beating rate (76 ± 1 versus 94 bpm; Figure 6B and 6C), delayed beating rate response (τ_{on} , 3.6 ± 1.2 versus 1.6 s), and prolonged beating rate recovery (τ_{off} , 3.2 ± 0.5 versus 1.4 s; Figure 6D). Consistent with our experimental findings, the increase in Ca^{2+} transient amplitude of HFpEF models under isoproterenol stimulation was also smaller than that of the control (Figure S14B and S14C).

Next, we investigated the efficacy of targeting the remodeled membrane versus the Ca^{2+} clock of HFpEF SAN models in ameliorating the chronotropic response (Figure 6E and 6F). To accomplish this, membrane clock remodeling or Ca^{2+} clock remodeling of HFpEF SAN models were independently reversed (ie, returned to control model parameter values). The increase in beat-

ing rate under isoproterenol was attenuated in HFpEF SAN models when Ca^{2+} clock remodeling was targeted compared with when membrane clock remodeling was targeted (1.46 ± 0.21 bpm versus 19.66 ± 0.65 bpm); the beating rate of the control model increased by ≈ 20.2 bpm under isoproterenol. Both τ_{on} and τ_{off} fell to values comparable to that of control in HFpEF SAN models when membrane clock remodeling was targeted. Contrarily, both τ_{on} and τ_{off} remained significantly larger in HFpEF SAN models when Ca^{2+} clock remodeling was targeted (Figure 6F). In summary, targeting membrane clock remodeling in HFpEF SAN models ameliorated all aspects of chronotropic response but targeting Ca^{2+} clock remodeling did not.

In previous experiments, we sought to understand what would happen if an aspect of pathophysiologic remodeling was reversed. Next, however, we conducted a sensitivity analysis to determine how maximal beating rate under isoproterenol changed with respect to each individual membrane clock and Ca^{2+} clock parameters across all HFpEF SAN models (Figure 6G). We chose to focus on submaximal beating rate as the presentation of chronotropic incompetence to treat because it is one of the standard metrics used to diagnose patients in the clinic.²² The magnitude and sign of a sensitivity coefficient indicate the degree of change and its correlation between beating rate and a specific parameter. We found that the parameters k_{dL} (I_{CaL} activation kinetics) and g_f (funny current conductance) had the largest impacts on maximal beating rate under isoproterenol (0.98 ± 0.02 and 0.15 ± 0.02 , respectively). Consistent with our previous simulation results, changes to the membrane clock are associated with changes in maximum beating rate under isoproterenol. Moreover, these results suggest that I_{CaL} would be a particularly promising therapeutic target for treating chronotropic incompetence.

DISCUSSION

HFpEF is now regarded as a systemic syndrome that goes beyond left ventricular diastolic dysfunction.² Although the pathophysiology of chronotropic incompetence associated with exercise intolerance remains uncertain, it is a cardinal feature of human HFpEF. By investigating the mechanisms underlying the limited chronotropic response in HFpEF animal models, we identified SAN

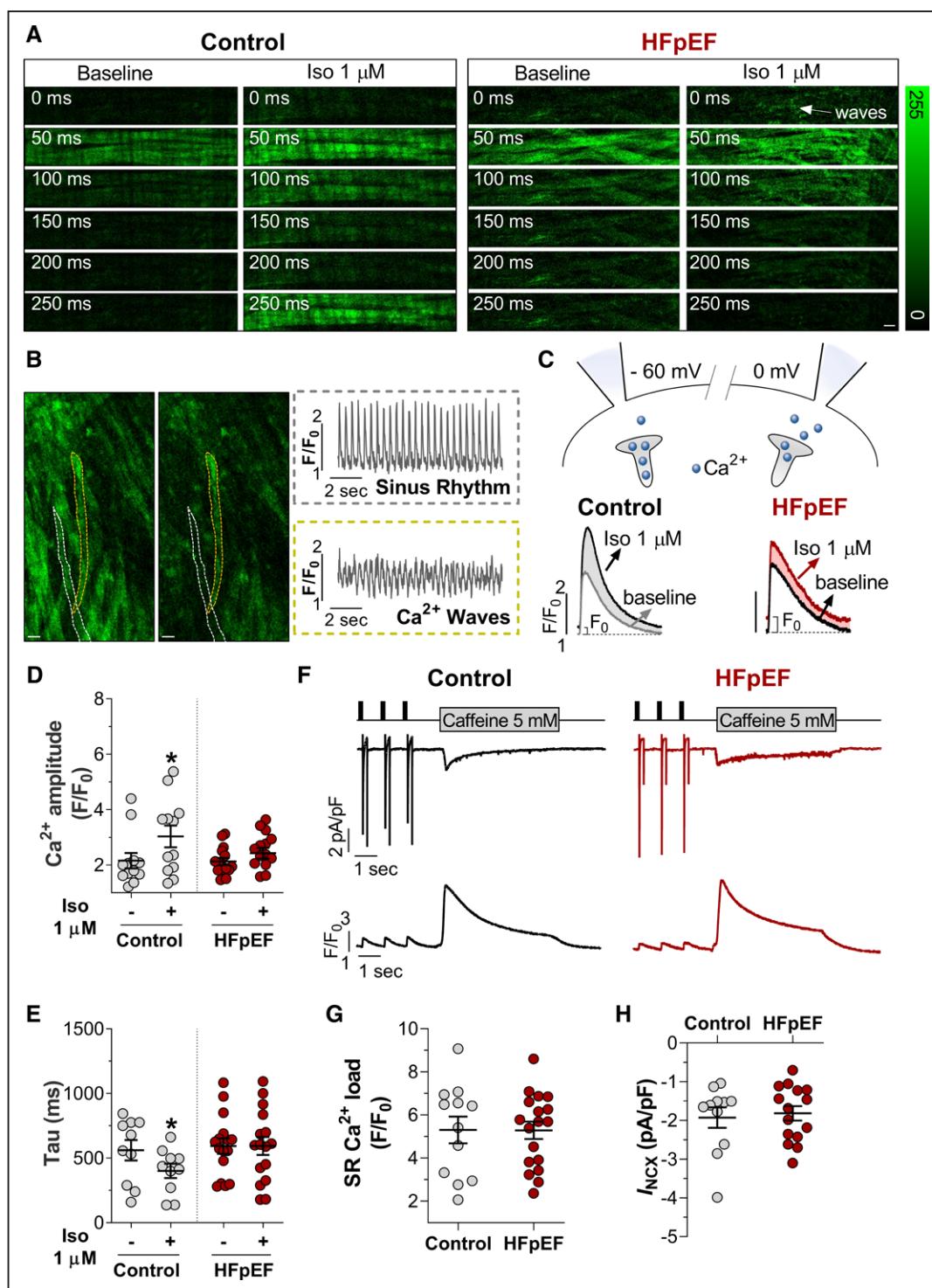


Figure 5. Compromised intracellular Ca²⁺ transients in SAN of HFpEF.

A, Time series of 2D confocal images of pacemaker cells within the intact SAN (scale bar, 60 μ m). **B**, A still frame from a 2D confocal image of Ca²⁺ fluorescence in a wide field of the explanted HFpEF SAN tissue, showing 2 neighbor cells: 1 under intrinsic sinus rhythm (marked by white dashed lines), and 1 with Ca²⁺ waves (marked by yellow dashed lines); scale bar, 20 μ m. **B, Right**, The differential oscillatory pattern. **C**, Membrane depolarization-induced global cytosolic Ca²⁺ transient (**top**) and representative Ca²⁺ transient in control and HFpEF SAN cells under baseline and Iso stimulation (**bottom**). **D**, Mean Ca²⁺ transient amplitude. **E**, Mean time constant of Ca²⁺ decay (Tau). **F**, Representative tracings of application of a caffeine solution after pacing to steady state at 1 Hz provided a measurement of caffeine-induced inward NCX current and SR load. **G**, Mean SR Ca²⁺ load. **H**, Mean peak NCX current (I_{NCX}). Mean values were obtained from control (n=10–12 cells from 3 animals) and HFpEF (n=15–18 cells from 3 animals). Data are expressed as mean \pm SEM. Repeated measures ANOVA followed by Bonferroni post hoc test (**D** and **E**). Unpaired Student *t* test (**G** and **H**). **P*<0.05. HFpEF indicates heart failure with preserved ejection fraction; Iso, isoproterenol; NCX, Na⁺/Ca²⁺ exchanger; SAN, sinoatrial node; and SR, sarcoplasmic reticulum.

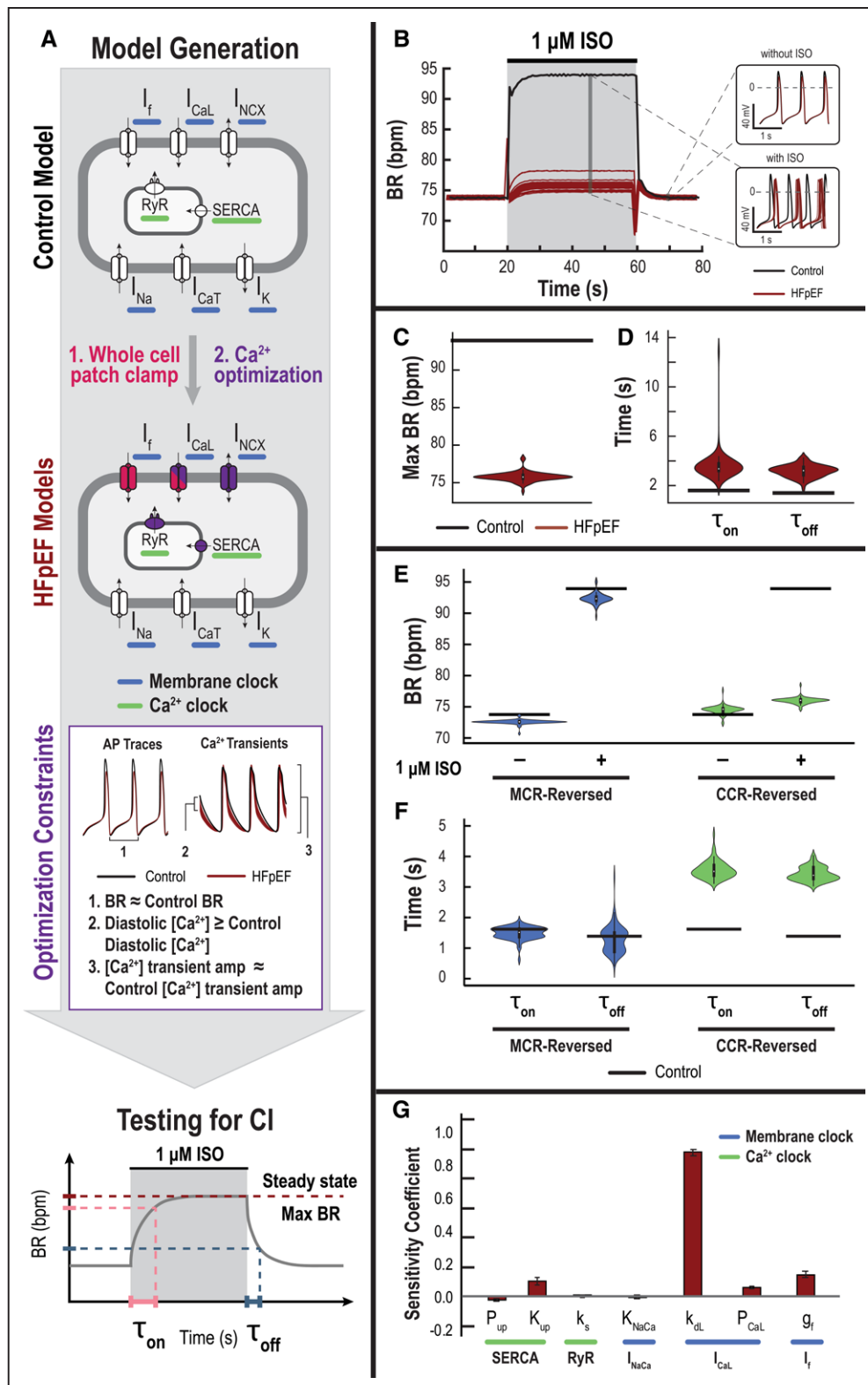


Figure 6. Computer simulations reveal the dominant role of HFpEF-associated membrane clock remodeling on the impaired sinoatrial node β -adrenergic receptor responsiveness.

A, Computer simulation workflow. Incorporation of ionic remodeling into biophysically detailed human sinoatrial node membrane kinetic model (top). First, ionic remodeling of the MC (80% and 34% reduction in funny current and L-type Ca^{2+} current conductances) was incorporated (pink). Subsequently, additional Ca^{2+} handling parameters (SERCA, RyR, L-type Ca^{2+}) were tuned so that the resultant HFpEF models recapitulated changes in experimental Ca^{2+} transient dynamics. When testing for CI (bottom), models were challenged with a 40-s pulse of 1 $\mu\text{mol/L}$ ISO; maximal BR, BR response (τ_{on}), and BR recovery (τ_{off}) were quantified. **B**, Instantaneous BR plotted vs time for control (Continued)

Figure 6 Continued. (black) and HFpEF (red) models subject to a 40-s 1- μ mol/L ISO pulse; representative action potentials (left) for control (black) and collection of HFpEF (red) sinoatrial node models with and without ISO (inset). Violin plots of **(C)** maximum BRs, and **(D)** BR response (τ_{on} , left) and BR recovery (τ_{off} , right) of HFpEF models subject to 1- μ mol/L ISO pulse; black horizontal lines indicate corresponding control values. **E** and **F**, Contributions of MC and CC remodeling to CI. **E**, Steady-state BRs with and without ISO. **F**, BR response (τ_{on} , left) and BR recovery (τ_{off} , right) of models with either MC remodeling (blue) or CC remodeling (green); horizontal black bars indicate control model dynamics. **G**, Bar graph of sensitivity coefficients of membrane and calcium clock parameters. The sensitivity coefficients represent how changes in each of these parameters affect BR. BR indicates beating rate; I_{CaL} , Ca^{2+} current, L-type; I_{CaT} , Ca^{2+} current, L-type; CC, calcium clock; CCR, Ca^{2+} clock remodeling; CI, chronotropic incompetence; I_f , funny current; HFpEF, heart failure with preserved ejection fraction; ISO, isoproterenol; MC, membrane clock; MCR, membrane clock remodeling; Na, sodium; K, potassium; NCX, Na^+/Ca^{2+} exchanger; RyR, ryanodine receptor; and SERCA, sarco(endo)plasmic reticulum Ca^{2+} -ATPase.

dysfunction induced by stress. Our integrated approach revealed evidence of chronotropic incompetence in both types of HF (HFrEF and HFpEF), and carefully characterized functional, structural, and molecular features underlying the defective SAN function in HFpEF.

Although autonomic and endothelial dysfunction¹ and lower cardiopulmonary reserve⁴⁰ are critical components of exercise intolerance in HFpEF patients, here we expand the current knowledge proposing SAN dysfunction as a new component contributing to the impaired exercise tolerance in HFpEF.³ Our findings demonstrate impaired cardiac output reserve in HFpEF, which has been shown to be a critical determinant of exercise intolerance in HFpEF patients.⁴¹ Disease-associated SAN dysfunction has been described in many heart conditions,^{7–9,42} but has not been examined in HFpEF. Studies in human, canine, and mouse SAN demonstrated that maladaptive structural remodeling in heart disease with SAN dysfunction leads to anatomic obstacles favoring conduction abnormalities.^{7,23,28} Moreover, increased SAN fibrosis may create additional insulation layers in the SAN pacemaker complex, which can impair the synchronization of different pacemaker clusters, thereby facilitating multiple leading pacemakers.^{7,23,28} Thus, source–sink mismatch and inadequate SAN redundancies essential for protecting heart rhythmicity predispose the SAN dysfunction in HFpEF, by which lethal arrhythmias could occur.^{18,43} Supporting the H₂FPEF⁴⁴ and HFA-PEFF⁴⁵ diagnostic scores, our findings advocate for exercise testing to unmask chronotropic incompetence and facilitate HFpEF diagnosis.

Multiple animal models of HFpEF have been developed⁴⁶ and faithfully recapitulate critical features of human diseases.^{14,17,19–21} Taking into consideration that hypertension is one of the most prevailing risk factors in patients with sick sinus syndrome,⁴⁷ the remarkable hypertensive feature of the DSS rat HFpEF model coincides with the high prevalence in human HFpEF.² This rat model also has insulin resistance and hyperlipidemia,^{15,16} further increasing its relevance to human HFpEF. Moreover, we recently reported impaired SAN function using a HFpEF model that replicates the chronological development of this disease and the epidemiological evidence of sex-related distribution.⁴⁸ In addition, our results were partially replicated in the recently described 2-hit model of HFpEF. Taken together, these findings suggest that chronotropic incompetence is a

common condition associated with HF caused by intrinsic SAN dysfunction in HFpEF.

The current view of spontaneous cardiac pacemaking activity relies on the synchronous function of voltage-dependent ion channels (named membrane clock) coupled to a Ca^{2+} clock, generating highly interdependent and synchronic oscillations.³⁴ However, the diversity of cell types populating the leading SAN region gives an extra, yet decisive, structural complexity that goes beyond its fibrotic insulation. Multiple intranodal pacemakers have different sensitivity to physiological and pathological stimulations,⁴⁹ which are fundamental to maintaining SAN robustness, especially during fight-or-flight response needs.^{23,48} The coexistence of similar, but not identical, pacemaker cells within the SAN and surrounding working atrial myocardium has been proposed,^{25,26,49} and these observations might be justified by differential mRNA cargos of SAN pacemaker cells.^{29,30} Although shifts in the molecular signature of SAN toward transitional cells seem not to be responsible for the SAN dysfunction in HFpEF, enrichment of gene clusters related to oxidative stress and inflammation may further amplify the severity of the disease.^{50,51} While transcriptome profiling at single-cell resolution has provided a molecular transcriptome atlas of SAN tissue at the embryonic stage,^{29,30} the challenges imposed by adult stages (eg, low and variable yield of viable pacemaker cells, irregular shape, and large cell size) represent a technical limitation of the present study.

Given the vital importance of adequate β -AR response, multiple components of the pacemaking machinery exert clear and quantifiable contributions to maintain and/or accelerate the HR, while the loss of these components impairs the proper regulation of rate response.^{28,34} Depressed expression and function of the membrane clock components may account for the reduced chronotropic reserve in HFpEF, which has also been linked to SAN dysfunction in transgenic mice lacking $Ca_v1.3$ or $Hcn4$.^{52,53} The role of $Hcn4$ channel has been investigated in HFpEF, where it was hypothesized that prolonging diastole can favor complete myocardial relaxation, thereby leading to decreased filling pressures.⁵⁴ However, ivabradine, a selective inhibitor of I_f , failed to improve diastolic function and exercise tolerance in HFpEF patients.^{55,56} Our results further question the rationale for ivabradine in HFpEF. Interestingly, despite the presence of chronotropic incompetence in

HFrEF, ivabradine has proven to be beneficial in HFrEF patients in the absence of bradycardia.⁵⁷ Distinct mechanisms of chronotropic incompetence and SAN dysfunction in different forms of HF may account for these differences. Thus, the identification of unique molecular signatures of SAN dysfunction in HFrEF and HFpEF warrants further investigation.

In summary, exercise intolerance and limited chronotropic response in HFpEF are associated with functional, structural, and molecular remodeling of the SAN leading to defective fail-safe mechanisms. Impaired SAN robustness in HFpEF is characterized by reduced chronotropic response to β -AR stimulation and uncoordinated recruitment of pacemaker clusters under stress conditions that favor rhythmic abnormalities.

Limitations and Perspectives

Some limitations of the present study should be noted. First, although we showed concordant findings from 2 distinct HFpEF models, the limitations of translating the findings to humans were recently discussed² and support the need for improved preclinical models. Second, although this study provides granular details of mechanisms responsible for SAN dysfunction, we did not establish a direct link to exercise intolerance. Despite these limitations, the present study brings novel mechanistic insights into SAN dysfunction in HFpEF. Future studies are needed to establish the potential role of novel specific therapies to target this condition.

ARTICLE INFORMATION

Received March 26, 2021; accepted November 9, 2021.

Affiliations

Smidt Heart Institute, Cedars-Sinai Medical Center, Los Angeles, CA (T.M., R.Z., J.H.C., R.Z., Y.N.L., L.S., J.I.G., W.L., E.C.). Department of Biomedical Engineering (J.K.Y., J.A.L., N.A.T.) and Alliance for Cardiovascular and Diagnostic and Treatment Innovation (N.A.T.), Johns Hopkins University, Baltimore, MD.

Acknowledgments

The authors thank Eduardo Marbán for numerous helpful discussions, Lisa Trahan for editorial assistance, and Catherine Bresee for statistical consultation.

Sources of Funding

This research was supported by National Institutes of Health (grants R01 HL135866 and R01 HL147570 to Dr Cingolani; grants R01 HL142496, R01 HL126802, and U01HL141074 to Dr Trayanova), a Leducq Foundation award (to Dr Trayanova), the Peer-Reviewed Medical Research Program of the US Department of Defense (PR150620), the American Heart Association (836665 to Dr Mesquita), and the Cedars-Sinai Board of Governors.

Disclosures

None.

Supplemental Material

Supplemental Methods
Tables S1–S9
Figures S1–S15
Videos S1–S4
References 58–62

REFERENCES

- Borlaug BA, Melenovsky V, Russell SD, Kessler K, Pacak K, Becker LC, Kass DA. Impaired chronotropic and vasodilator reserves limit exercise capacity in patients with heart failure and a preserved ejection fraction. *Circulation*. 2006;114:2138–2147. doi: 10.1161/CIRCULATIONAHA.106.632745
- Shah SJ, Borlaug BA, Kitzman DW, McCulloch AD, Blaxall BC, Agarwal R, Chirinos JA, Collins S, Deo RC, Gladwin MT, et al. Research priorities for heart failure with preserved ejection fraction: National Heart, Lung, and Blood Institute Working Group summary. *Circulation*. 2020;141:1001–1026. doi: 10.1161/CIRCULATIONAHA.119.041886
- Sarma S, Stoller D, Hendrix J, Howden E, Lawley J, Livingston S, Adams-Huet B, Holmes C, Goldstein DS, Levine BD. Mechanisms of chronotropic incompetence in heart failure with preserved ejection fraction. *Circ Heart Fail*. 2020;13:e006331. doi: 10.1161/CIRCHEARTFAILURE.119.006331
- Borlaug BA, Kane GC, Melenovsky V, Olson TP. Abnormal right ventricular-pulmonary artery coupling with exercise in heart failure with preserved ejection fraction. *Eur Heart J*. 2016;37:3293–3302. doi: 10.1093/eurheartj/ehw241
- Borlaug BA, Nishimura RA, Sorajja P, Lam CS, Redfield MM. Exercise hemodynamics enhance diagnosis of early heart failure with preserved ejection fraction. *Circ Heart Fail*. 2010;3:588–595. doi: 10.1161/CIRCHEARTFAILURE.109.930701
- Del Buono MG, Arena R, Borlaug BA, Carbone S, Canada JM, Kirkman DL, Garten R, Rodriguez-Miguel P, Guazzi M, Lavie CJ, et al. Exercise intolerance in patients with heart failure: JACC State-of-the-Art review. *J Am Coll Cardiol*. 2019;73:2209–2225. doi: 10.1016/j.jacc.2019.01.072
- Lou Q, Hansen BJ, Fedorenko O, Csepe TA, Kalyanasundaram A, Li N, Hage LT, Glukhov AV, Billman GE, Weiss R, et al. Upregulation of adenosine A1 receptors facilitates sinoatrial node dysfunction in chronic canine heart failure by exacerbating nodal conduction abnormalities revealed by novel dual-sided intramural optical mapping. *Circulation*. 2014;130:315–324. doi: 10.1161/CIRCULATIONAHA.113.007086
- Soltysinska E, Speersneider T, Winther SV, Thomsen MB. Sinoatrial node dysfunction induces cardiac arrhythmias in diabetic mice. *Cardiovasc Diabetol*. 2014;13:122. doi: 10.1186/s12933-014-0122-y
- Yanni J, Tellez JO, Maczewski M, Mackiewicz U, Beresewicz A, Billeter R, Dobrzynski H, Boyett MR. Changes in ion channel gene expression underlying heart failure-induced sinoatrial node dysfunction. *Circ Heart Fail*. 2011;4:496–508. doi: 10.1161/CIRCHEARTFAILURE.110.957647
- Sanders P, Kistler PM, Morton JB, Spence SJ, Kalman JM. Remodeling of sinus node function in patients with congestive heart failure: reduction in sinus node reserve. *Circulation*. 2004;110:897–903. doi: 10.1161/01.CIR.0000139336.69955.AB
- Cingolani E, Goldhaber JL, Marbán E. Next-generation pacemakers: from small devices to biological pacemakers. *Nat Rev Cardiol*. 2018;15:139–150. doi: 10.1038/nrcardio.2017.165
- John RM, Kumar S. Sinus node and atrial arrhythmias. *Circulation*. 2016;133:1892–1900. doi: 10.1161/CIRCULATIONAHA.116.018011
- Zakeri R, Chamberlain AM, Roger VL, Redfield MM. Temporal relationship and prognostic significance of atrial fibrillation in heart failure patients with preserved ejection fraction: a community-based study. *Circulation*. 2013;128:1085–1093. doi: 10.1161/CIRCULATIONAHA.113.001475
- Gallet R, de Couto G, Simsolo E, Valle J, Sun B, Liu W, Tseliou E, Zile MR, Marbán E. Cardiosphere-derived cells reverse heart failure with preserved ejection fraction (HFpEF) in rats by decreasing fibrosis and inflammation. *JACC Basic Transl Sci*. 2016;1:14–28. doi: 10.1016/j.jacbs.2016.01.003
- Wendt N, Schulz A, Qadri F, Bolbrinker J, Kossmehl P, Winkler K, Stoll M, Vetter R, Kreutz R. Genetic analysis of salt-sensitive hypertension in Dahl rats reveals a link between cardiac fibrosis and high cholesterol. *Cardiovasc Res*. 2009;81:618–626. doi: 10.1093/cvr/cvn263
- Reaven GM, Twersky J, Chang H. Abnormalities of carbohydrate and lipid metabolism in Dahl rats. *Hypertension*. 1991;18:630–635. doi: 10.1161/01.hyp.18.5.630
- Cho JH, Zhang R, Kilfoil PJ, Gallet R, de Couto G, Bresee C, Goldhaber JL, Marbán E, Cingolani E. Delayed repolarization underlies ventricular arrhythmias in rats with heart failure and preserved ejection fraction. *Circulation*. 2017;136:2037–2050. doi: 10.1161/CIRCULATIONAHA.117.028202
- Cho JH, Zhang R, Aynaszyan S, Holm K, Goldhaber JL, Marbán E, Cingolani E. Ventricular arrhythmias underlie sudden death in rats with heart failure and preserved ejection fraction. *Circ Arrhythm Electrophysiol*. 2018;11:e006452. doi: 10.1161/CIRCEP.118.006452
- Schiattarella GG, Altamirano F, Tong D, French KM, Villalobos E, Kim SY, Luo X, Jiang N, May HL, Wang ZV, et al. Nitrosative stress drives heart

- failure with preserved ejection fraction. *Nature*. 2019;568:351–356. doi: 10.1038/s41586-019-1100-z
20. Tong D, Schiattarella GG, Jiang N, Altamirano F, Szweda PA, Elnwasany A, Lee DI, Yoo H, Kass DA, Szweda LI, et al. NAD⁺ repletion reverses heart failure with preserved ejection fraction. *Circ Res*. 2021;128:1629–1641. doi: 10.1161/CIRCRESAHA.120.317046
 21. Schiattarella GG, Altamirano F, Kim SY, Tong D, Ferdous A, Piristine H, Dasgupta S, Wang X, French KM, Villalobos E, et al. Xbp1s-FoxO1 axis governs lipid accumulation and contractile performance in heart failure with preserved ejection fraction. *Nat Commun*. 2021;12:1684. doi: 10.1038/s41467-021-21931-9
 22. Zweerink A, van der Lingen ACJ, Handoko ML, van Rossum AC, Allaart CP. Chronotropic incompetence in chronic heart failure. *Circ Heart Fail*. 2018;11:e004969. doi: 10.1161/CIRCHEARTFAILURE.118.004969
 23. Li N, Hansen BJ, Csepe TA, Zhao J, Ignozzi AJ, Sul LV, Zakharkin SO, Kalyanasundaram A, Davis JP, Biesiadecki BJ, et al. Redundant and diverse intranodal pacemakers and conduction pathways protect the human sinoatrial node from failure. *Sci Transl Med*. 2017;9:eaa5607. doi: 10.1126/scitranslmed.aam5607
 24. Ungerer M, Böhm M, Elce JS, Erdmann E, Lohse MJ. Altered expression of beta-adrenergic receptor kinase and beta 1-adrenergic receptors in the failing human heart. *Circulation*. 1993;87:454–463. doi: 10.1161/01.cir.87.2.454
 25. Boyett MR, Honjo H, Kodama I. The sinoatrial node, a heterogeneous pacemaker structure. *Cardiovasc Res*. 2000;47:658–687. doi: 10.1016/s0008-6363(00)00135-8
 26. Fedorov VV, Schuessler RB, Hemphill M, Ambrosi CM, Chang R, Voloshina AS, Brown K, Hucker WJ, Efimov IR. Structural and functional evidence for discrete exit pathways that connect the canine sinoatrial node and atria. *Circ Res*. 2009;104:915–923. doi: 10.1161/CIRCRESAHA.108.193193
 27. Cho JH, Kilfoil PJ, Zhang R, Solymani RE, Bresee C, Kang EM, Luther K, Rogers RG, de Couto G, Goldhaber JL, et al. Reverse electrical remodeling in rats with heart failure and preserved ejection fraction. *JCI Insight*. 2018;3:121123. doi: 10.1172/jci.insight.121123
 28. Glukhov AV, Kalyanasundaram A, Lou G, Hage LT, Hansen BJ, Belevych AE, Mohler PJ, Knollmann BC, Periasamy M, Györke S, et al. Caldesmon 2 deletion causes sinoatrial node dysfunction and atrial arrhythmias associated with altered sarcoplasmic reticulum calcium cycling and degenerative fibrosis within the mouse atrial pacemaker complex1. *Eur Heart J*. 2015;36:686–697. doi: 10.1093/eurheartj/ehf452
 29. Goodyer WR, Beyersdorf BM, Paik DT, Tian L, Li G, Buikema JW, Chirikian O, Choi S, Venkatraman S, Adams EL, et al. Transcriptomic profiling of the developing cardiac conduction system at single-cell resolution. *Circ Res*. 2019;125:379–397. doi: 10.1161/CIRCRESAHA.118.314578
 30. van Eif VWW, Stefanovic S, van Duijnenboden K, Bakker M, Wakker V, de Gier-de Vries C, Zaffran S, Verkerk AO, Boukens BJ, Christoffels VM. Transcriptome analysis of mouse and human sinoatrial node cells reveals a conserved genetic program. *Development*. 2019;146:dev173161. doi: 10.1242/dev.173161
 31. Mangoni ME, Couette B, Bourinet E, Platzer J, Reimer D, Striessnig J, Nargeot J. Functional role of L-type Cav1.3 Ca²⁺ channels in cardiac pacemaker activity. *Proc Natl Acad Sci U S A*. 2003;100:5543–5548. doi: 10.1073/pnas.0935295100
 32. Mangoni ME, Traboulsie A, Leoni AL, Couette B, Marger L, Le Quang K, Kupfer E, Cohen-Solal A, Vilar J, Shin HS, et al. Bradycardia and slowing of the atrioventricular conduction in mice lacking Cav3.1/alpha1G T-type calcium channels. *Circ Res*. 2006;98:1422–1430. doi: 10.1161/01.RES.0000225862.14314.49
 33. Ono K, Iijima T. Pathophysiological significance of T-type Ca²⁺ channels: properties and functional roles of T-type Ca²⁺ channels in cardiac pacemaking. *J Pharmacol Sci*. 2005;99:197–204. doi: 10.1254/jphs.fmj05002x2
 34. Tsutsui K, Monfredi OJ, Sirenko-Tagirova SG, Maltseva LA, Bychkov R, Kim MS, Ziman BD, Tarasov KV, Tarasova YS, Zhang J, et al. A coupled-clock system drives the automaticity of human sinoatrial nodal pacemaker cells. *Sci Signal*. 2018;11:eaa67608. doi: 10.1126/scisignal.aap67608
 35. Torrente AG, Zhang R, Zaini A, Giani JF, Kang J, Lamp ST, Philipson KD, Goldhaber JL. Burst pacemaker activity of the sinoatrial node in sodium-calcium exchanger knockout mice. *Proc Natl Acad Sci U S A*. 2015;112:9769–9774. doi: 10.1073/pnas.1505670112
 36. Torrente AG, Fossier L, Baudot M, Bidaud I, Mesirca P, Mangoni M. Role of L-type Cav1.3 Ca²⁺ channels in Ca²⁺ handling and SAN pacemaker activity altered by external conditions. *Arch Cardiovasc Dis Suppl*. 2018;10:241. doi: 10.1016/j.acvdsp.2018.02.143
 37. Verkerk AO, van Borren MM, van Ginneken AC, Wilders R. Ca(2+) cycling properties are conserved despite bradycardic effects of heart failure in sinoatrial node cells. *Front Physiol*. 2015;6:18. doi: 10.3389/fphys.2015.00018
 38. Verkerk AO, Wilders R, Coronel R, Ravensloot JH, Verheijck EE. Ionic remodeling of sinoatrial node cells by heart failure. *Circulation*. 2003;108:760–766. doi: 10.1161/01.CIR.0000083719.51661.B9
 39. Fabbri A, Fantini M, Wilders R, Severi S. Computational analysis of the human sinus node action potential: model development and effects of mutations. *J Physiol*. 2017;595:2365–2396. doi: 10.1113/JP273259
 40. Gorter TM, Obokata M, Reddy YNV, Melenovsky V, Borlaug BA. Exercise unmasks distinct pathophysiological features in heart failure with preserved ejection fraction and pulmonary vascular disease. *Eur Heart J*. 2018;39:2825–2835. doi: 10.1093/eurheartj/ehy331
 41. Obokata M, Kane GC, Reddy YN, Olson TP, Melenovsky V, Borlaug BA. Role of diastolic stress testing in the evaluation for heart failure with preserved ejection fraction: a simultaneous invasive-echocardiographic study. *Circulation*. 2017;135:825–838. doi: 10.1161/CIRCULATIONAHA.116.024822
 42. Neco P, Torrente AG, Mesirca P, Zorio E, Liu N, Priori SG, Napolitano C, Richard S, Benitah JP, Mangoni ME, et al. Paradoxical effect of increased diastolic Ca(2+) release and decreased sinoatrial node activity in a mouse model of catecholaminergic polymorphic ventricular tachycardia. *Circulation*. 2012;126:392–401. doi: 10.1161/CIRCULATIONAHA.111.075382
 43. Vaduganathan M, Patel RB, Michel A, Shah SJ, Senni M, Gheorghiadu M, Butler J. Mode of death in heart failure with preserved ejection fraction. *J Am Coll Cardiol*. 2017;69:556–569. doi: 10.1016/j.jacc.2016.10.078
 44. Reddy YNV, Carter RE, Obokata M, Redfield MM, Borlaug BA. A simple, evidence-based approach to help guide diagnosis of heart failure with preserved ejection fraction. *Circulation*. 2018;138:861–870. doi: 10.1161/CIRCULATIONAHA.118.034646
 45. Pieske B, Tschöpe C, de Boer RA, Fraser AG, Anker SD, Donal E, Edelmann F, Fu M, Guazzi M, Lam CSP, et al. How to diagnose heart failure with preserved ejection fraction: the HFA-PEFF diagnostic algorithm: a consensus recommendation from the Heart Failure Association (HFA) of the European Society of Cardiology (ESC). *Eur J Heart Fail*. 2020;22:391–412. doi: 10.1002/ehf.1741
 46. Valero-Muñoz M, Backman W, Sam F. Murine models of heart failure with preserved ejection fraction: a "fishing expedition". *JACC Basic Transl Sci*. 2017;2:770–789. doi: 10.1016/j.jaccbts.2017.07.013
 47. Jensen PN, Gronroos NN, Chen LY, Folsom AR, deFilippi C, Heckbert SR, Alonso A. Incidence of and risk factors for sick sinus syndrome in the general population. *J Am Coll Cardiol*. 2014;64:531–538. doi: 10.1016/j.jacc.2014.03.056
 48. Mesquita TRR, Zhang R, de Couto G, Valle J, Sanchez L, Rogers RG, Holm K, Liu W, Marbán E, Cingolani E. Mechanisms of atrial fibrillation in aged rats with heart failure with preserved ejection fraction. *Heart Rhythm*. 2020;17:1025–1033. doi: 10.1016/j.hrthm.2020.02.007
 49. Kim MS, Maltsev AV, Monfredi O, Maltseva LA, Wirth A, Florio MC, Tsutsui K, Riordon DR, Parsons SP, Tagirova S, et al. Heterogeneity of calcium clock functions in dormant, dysrhythmically and rhythmically firing single pacemaker cells isolated from SA node. *Cell Calcium*. 2018;74:168–179. doi: 10.1016/j.ceca.2018.07.002
 50. Swaminathan PD, Purohit A, Soni S, Voigt N, Singh MV, Glukhov AV, Gao Z, He BJ, Luczak ED, Joiner ML, et al. Oxidized CaMKII causes cardiac sinus node dysfunction in mice. *J Clin Invest*. 2011;121:3277–3288. doi: 10.1172/JCI57833
 51. Leuschner F, Nahrendorf M. Novel functions of macrophages in the heart: insights into electrical conduction, stress, and diastolic dysfunction. *Eur Heart J*. 2020;41:989–994. doi: 10.1093/eurheartj/ehz159
 52. Baruscotti M, Bucchi A, Visconti C, Mandelli G, Consalez G, Gneschi-Rusconi T, Montano N, Casali KR, Micheloni S, Barbuti A, et al. Deep bradycardia and heart block caused by inducible cardiac-specific knockout of the pacemaker channel gene Hcn4. *Proc Natl Acad Sci U S A*. 2011;108:1705–1710. doi: 10.1073/pnas.1010122108
 53. Platzer J, Engel J, Schrott-Fischer A, Stephan K, Bova S, Chen H, Zheng H, Striessnig J. Congenital deafness and sinoatrial node dysfunction in mice lacking class D L-type Ca²⁺ channels. *Cell*. 2000;102:89–97. doi: 10.1016/s0092-8674(00)00013-1
 54. Reil JC, Hohl M, Reil GH, Granzier HL, Kratz MT, Kazakov A, Fries P, Müller A, Lenski M, Custodis F, et al. Heart rate reduction by If-inhibition improves vascular stiffness and left ventricular systolic and diastolic function in a mouse model of heart failure with preserved ejection fraction. *Eur Heart J*. 2013;34:2839–2849. doi: 10.1093/eurheartj/ehs218

55. Pal N, Sivaswamy N, Mahmod M, Yavari A, Rudd A, Singh S, Dawson DK, Francis JM, Dwight JS, Watkins H, et al. Effect of selective heart rate slowing in heart failure with preserved ejection fraction. *Circulation*. 2015;132:1719–1725. doi: 10.1161/CIRCULATIONAHA.115.017119
56. Komajda M, Isnard R, Cohen-Solal A, Metra M, Pieske B, Ponikowski P, Voors AA, Dominjon F, Henon-Goburdhun C, Pannaux M, et al; Preserved Left Ventricular Ejection Fraction Chronic Heart Failure with Ivabradine Study (EDIFY) Investigators. Effect of ivabradine in patients with heart failure with preserved ejection fraction: the EDIFY randomized placebo-controlled trial. *Eur J Heart Fail*. 2017;19:1495–1503. doi: 10.1002/ejhf.876
57. Bouabdallaoui N, O'Meara E, Bernier V, Komajda M, Swedberg K, Tavazzi L, Borer JS, Bohm M, Ford I, Tardif JC. Beneficial effects of ivabradine in patients with heart failure, low ejection fraction, and heart rate above 77 b.p.m. *ESC Heart Fail*. 2019;6:1199–1207. doi: 10.1002/ehf2.12513
58. Elkholey K, Morris L, Niewiadomska M, Houser J, Ramirez M, Tang M, Humphrey MB, Stavrakis S. Sex differences in the incidence and mode of death in rats with heart failure with preserved ejection fraction. *Exp Physiol*. 2021;106:673–682. doi: 10.1113/EP089163
59. Tong D, Schiattarella GG, Jiang N, May HI, Lavandro S, Gillette TG, Hill JA. Female sex is protective in a preclinical model of heart failure with preserved ejection fraction. *Circulation*. 2019;140:1769–1771. doi: 10.1161/CIRCULATIONAHA.119.042267
60. Laughner JI, Ng FS, Sulkin MS, Arthur RM, Efimov IR. Processing and analysis of cardiac optical mapping data obtained with potentiometric dyes. *Am J Physiol Heart Circ Physiol*. 2012;303:H753–H765. doi: 10.1152/ajpheart.00404.2012
61. Lagarias JC, Reeds JA, Wright MH, et al. Convergence properties of the Nelder–Mead simplex method in low dimensions. *SIAM J Optim*. 1998;9:112–147.
62. Severi S, Fantini M, Charawi LA, DiFrancesco D. An updated computational model of rabbit sinoatrial action potential to investigate the mechanisms of heart rate modulation. *J Physiol*. 2012;590:4483–4499. doi: 10.1113/jphysiol.2012.229435